OPEN ACCESS
IOP PUBLISHING
SCIENCE AND TECHNOLOGY OF ADVANCED MATERIALS
Sci. Technol. Adv. Mater. **14** (2013) 044401 (10pp)
doi:10.1088/1468-6996/14/4/044401

The influence of different nanostructured scaffolds on fibroblast growth

I-Cheng Chung[1], Ching-Wen Li[2] and Gou-Jen Wang[1,2,3]

[1] Graduate Institute of Biomedical Engineering, National Chung-Hsing University, Taichung 40227, Taiwan
[2] PhD Program in Tissue Engineering and Regenerative Medicine, National Chung-Hsing University, Taichung 40227, Taiwan
[3] Department of Mechanical Engineering, National Chung-Hsing University, Taichung 40227, Taiwan

Received 15 May 2013
Accepted for publication 15 May 2013
Published 18 July 2013
Online at stacks.iop.org/STAM/14/044401

Abstract
Skin serves as a protective barrier, modulating body temperature and waste discharge. It is therefore desirable to be able to repair any damage that occurs to the skin as soon as possible. In this study, we demonstrate a relatively easy and cost-effective method for the fabrication of nanostructured scaffolds, to shorten the time taken for a wound to heal. Various scaffolds consisting of nanohemisphere arrays of poly(lactic-co-glycolic acid) (PLGA), polylactide and chitosan were fabricated by casting using a nickel (Ni) replica mold. The Ni replica mold is electroformed using the highly ordered nanohemisphere array of the barrier-layer surface of an anodic aluminum oxide membrane as the template. Mouse fibroblast cells (L929s) were cultured on the nanostructured polymer scaffolds to investigate the effect of these different nanohemisphere arrays on cell proliferation. The concentration of collagen type I on each scaffold was then measured through enzyme-linked immunosorbent assay to find the most effective scaffold for shortening the wound-healing process. The experimental data indicate that the proliferation of L929 is superior when a nanostructured PLGA scaffold with a feature size of 118 nm is utilized.

Keywords: nanostructured scaffold, nanomolding, PLGA, mouse fibroblast cell

1. Introduction

Skin is a relatively soft tissue that covers the entire external surface of the human body and constitutes about 8% of the total body mass. Since skin serves a multitude of important bodily functions, it is vital that any damage to it is repaired as quickly as possible [1]. Dressings for skin wounds are in high demand because millions of people are prone to dermal injuries, which are caused by fire, heat, electricity, chemicals, UV light, nuclear radiation or diseases every year [2]. However, there has never been any report of a completely effective wound-healing treatment for reducing scars. The wound-healing process can be divided into four steps. These include coagulation and hemostasis, inflammation, proliferation and wound remodeling [3]. The first two steps can prevent the enlargement of the wound and bacterial infection, while proliferation and wound remodeling can manipulate the skin functionally and keep the wound esthetically perfect. Therefore, controlling the proliferation of the skin cells and the extracellular matrix of these cells is a critical issue in skin-regeneration research.

In cell biology, it has been demonstrated that cell adhesion, proliferation, migration and differentiation can be manipulated using scaffolds of different nanostructures [1, 4]. Recent progress in nanofabrication techniques has enabled the production of a diverse array of nanostructures, on various biomaterials, for skin-regeneration applications. These include nanodot arrays, nanoporous structures, nanoparticles and nanofibers. It has been reported that nanostructures, in the form of nanodot arrays, are able to induce an apoptosis-like abnormality in NIH 3T3 cells [5]. Xia *et al* [6] demonstrated

that TiO_2 nanotubes can induce cell proliferation, alkaline phosphatase activity and the expression of osteogenic proteins to a greater extent, indicating that the topology of any nanostructured implants should be taken into consideration. Chandrasekaran *et al* [7] fabricated nanofibers of different diameters, to create different pore sizes in the composite scaffold, for skin regeneration. It has been determined that the nanostructures affect the behaviors of both somatic cells and stem cells [8]. Kukumberg *et al* [4] demonstrated that human mesenchymal stem cells, cultured on a nanostructured scaffold, could differentiate into endothelial-like cells for vascular repair. Park *et al* [9] have shown that the nanopore structure of polystyrene caused adipose-derived stem cells (ASCs) to differentiate into adipogenic cells, and that the ASCs were inclined to differentiate into osteogenic cells on nanopillar-structured scaffolds.

There are two types of approaches for the fabrication of nanostructures: top-down and bottom-up [10, 11]. In top-down fabrication, techniques such as lithography, writing or stamping are utilized to engrave or add aggregates of molecules to a surface. Soft lithography and dip-pen lithography are two of the most promising top-down approaches. Bottom-up methods use self-assembly processes to construct atoms or molecules into more complex assemblies, including atomic and molecular nanostructures at a surface [12]. Both the top-down and bottom-up approaches usually result in the production of a single nanodevice in one operation. For low-cost mass production, replica molding or imprinting methods, which transfer patterns from a hard mold onto thermoplastic substances having a low glass transition temperature, are desirable [13, 14]. In replica molding or imprinting, the robustness and durability of the replica molds are the main requirements for industrial applications. Several materials have been used as a mold material. Silicon (Si) has been employed due to its compatibility with the semiconductor-manufacturing process [15]. However, its brittleness and poor durability limit its application. Polyvinyl-chloride-based molds, which were duplicated from the original highly ordered silica ball array, have been used for ultraviolet (UV) nanoimprinting of a nanosphere array on silicon and polyethylene terephthalate substrates [16]. Anodic aluminum oxide (AAO) membranes, having nanosized porous arrays of regular hexagonal-shaped cells with straight columnar channels, have been utilized as templates for the fabrication of nanoring and nanocone arrays, hard polydimethylsiloxane nanopillar modes for UV nanoimprinting photonic crystal structure on gallium nitride substrates and orderly nanostructured poly(lactic-co-glycolic acid) (PLGA) scaffolds for tissue engineering [17–19]. Bulk metallic glass (BMG)-based molds, which were directly hot embossed using master molds of Si, Ni and AAO, have been employed to fabricate another amorphous sample of BMG [20]. The feature size of the BMG molds was determined by the pattern size of the master molds.

As mentioned above, the influence of nanostructure on cell behavior has been investigated by many studies. These reports place their emphasis on the importance of irregular nanostructures [21] or nanorods [22]. When compared with irregular nanostructures or nanorods, nanohemisphere arrays are much more uniform; therefore, the influence of surface roughness can be minimized. Furthermore, the consistency of surface morphology can enhance the credibility of the cell culture results. In this work, the influence of scaffolds, consisting of different nanohemisphere arrays on skin tissue regeneration, is investigated. A replica mold is fabricated by nickel (Ni) electroforming using the highly ordered nanohemisphere array of the barrier-layer surface of an AAO membrane as the master mold. The feature size of the nanohemispheres can be controlled by using different etching solutions for the anodic oxidation of aluminum (Al). Using the Ni replica mold, nanostructured tissue engineering scaffolds of PLGA, polylactide (PLA) and chitosan are fabricated by casting. During the wound-healing process, the fibroblast is involved in the proliferation and tissue remodeling steps and plays an import role in extracellular matrix (collagen, elastin, laminin and fibronectin) formation [1]. Because of this, mouse fibroblast cells (L929s) were cultured on the scaffolds to investigate the influence of the different nanohemisphere arrays on cell growth. Collage type I is then measured through enzyme-linked immunosorbent assay (ELISA) to determine the most suitable nanohemisphere array material that can most effectively enhance the construction of the extracellular matrix.

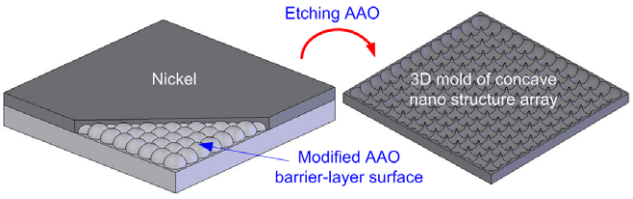

Figure 1. Schematic view of the proposed 3D nanoreplica mold.

2. Materials and methods

2.1. Nanostructured nickel mold preparation and characterization

Figure 1 shows a schematic illustration of the proposed three-dimensional (3D) structure of the nanoreplica mold. A modified AAO barrier-layer surface is used as the master mold for Ni thin film deposition. After etching the AAO template away, a 3D replica mold with a concave nanostructure array is obtained. The fabrication of the replica mold consisting of the nanohemisphere array entails the following: AAO film preparation, barrier-layer surface modification, Au thin film deposition, electrode annealing, device packaging and Ni electroforming. Since the Au thin film for the electrode is shaped by the structure of the surface of the barrier layer, the procedures involving the modification of the barrier-layer surface are critical. The detailed fabrication process is as follows:

1. *AAO film preparation*. The AAO films were fabricated by using an anodizing process. Al foils were cleaned with acetone, alcohol and de-ionized water several

times, and electropolished before anodization. AAO films, with nanopores having a diameter of 90 nm and thickness of 20–25 μm, were obtained by anodizing polished Al foil in an oxalic acid solution (0.3 M) under an applied voltage (50 V) at 0 °C for 5.5 h. When a phosphoric acid solution (0.1 M) under an applied voltage (150 V) at 0 °C for 6 h was employed, AAO films with a nanopore diameter of 300 nm are obtained. The remaining Al beneath the barrier layer was then dissolved in an aqueous $CuCl_2$–HCl solution that was prepared by dissolving powdered $CuCl_2$ (13.45 g) into a hydrochloric acid solution (100 ml, 35 wt%). A honeycomb-like barrier-layer surface was obtained after the removal of Al.

2. *Modification of the barrier-layer surface*. The honeycomb-like barrier-layer surface was placed into phosphoric acid (30 wt%) for 15 min to sharpen the shape of the hemisphere array for better electroforming. For the AAO films etched by phosphoric acid solution, the duration of this barrier-layer surface modification was increased to 45 min.
3. *Deposition of an Au thin film*. The modified barrier-layer surface was then used as the template for the deposition of an Au thin film (thickness approximately 30 nm) electrode by radio frequency magnetron sputtering (pressure = 3.9×10^{-3} Torr, temperature = room temperature, argon = 20 sccm, power = 80 W, processing time = 30 s).
4. *Annealing*. To further improve the conductivity of the Au thin film electrode, an additional annealing process was carried out. The annealing process consisted of heating the sample to 120 °C over a 20 min time frame, then holding at that temperature for 60 min and finally cooling in air to room temperature.
5. *Packaging*. Precise packaging before the electrochemical deposition of the Ni thin film ensures that the deposition occurs in the exact area required. The packaging procedure is as follows: adhere the AAO template on a glass substrate; fix an electric wire on the glass and connect the electric wire to the Au electrode on the AAO template using silver epoxy; and smear a thin layer of silica gel on the AAO master mold excluding the area for further Ni deposition, to restrict the deposition area.
6. *Nickel electroforming*. The electrodeposition process is as follows:
   (i) *Electrolyte preparation*. A sulfamate bath containing nickel aminosulfonate [$Ni(NH_2SO_3)_2 \times 4H_2O$)] and nickel chloride [$NiCl_4 \times 6H_2O$] in a boric acid solution [H_3BO_3] was used for electrodeposition. Since nickel sulfamate tetrahydrate possesses low internal stress and high solubility in water, the concentration of Ni ions in solution can be increased, thus enabling a higher rate of electrodeposition.
   (ii) *Measurement of effective electrode area*. Since the Ni thin film was deposited on the hemispheric electrode array, the effective area of the electrode could not be directly estimated by geometric analysis. The cyclic voltammetry (CV) method was used to determine the actual area of the Au thin film deposited on the AAO barrier-layer surface, which is used for the deposition of Ni thin film in this study. The device was dipped into a H_2SO_4 solution (0.5 M) for CV scanning (scanning rate = 100 mV s^{-1}, from 0.0 to 1.6 V). An electrochemical impedance spectroscopy instrument (SP-150, Bio-Logic, USA) was used for the CV tests.
   (iii) *Electroforming*. This was performed using a micro-electroforming system (EGG Instruments corporation/Model 263A) with a bulk Ni anode and the chromium- and Au-coated AAO barrier-layer surface as the cathode, under a constant current of 0.035 Å at a temperature of 55 °C. An Ni thin film is electrodeposited. The processing time depends on the desired thickness of the Ni film. After deposition, the AAO template was etched away by an NaOH solution (0.25 M) to obtain a replica mold of the nanohemisphere array.

The nanostructured topology of the AAO barrier layer and the Ni replica mold were characterized using scanning electron microscopy (SEM) and atomic force microscopy (AFM).

2.2. Nanostructured scaffold preparation and characterization

In this study, three materials, PLGA, PLA, which are synthetic, and chitosan, a natural polymer, were used as the scaffold materials. These materials are commonly used, FDA-approved, biodegradable materials with many useful biomedical applications [23]. The chemical structures of PLA and PLGA are similar. Chitosan is one of the most abundant biodegradable materials on earth. The details of how PLA, PLGA and chitosan are prepared for this study are described blow.

1. *PLGA solution preparation*. PLGA is a copolymer comprising lactic acid and glycolic acid. The ratio of lactide to glycolide used for polymerization (e.g. PLGA 75:25 denotes a copolymer whose composition is 75% lactic acid and 25% glycolic acid) determines the mechanical properties and biodegradability of a PLGA material.

The PLGA solution was prepared by dissolving 85/15 PLGA (IV:1.6–1.99 dl g^{-1}, M_w: 350 000–500 000 Da) (Green Squire Material Co, Ltd) in acetone at a w/w ratio of 1 : 4. The mixture was then stirred with a magnetic agitator for 60 min at 25 °C. The PLGA solution was then shaken in an ultrasonic shaker for 15 min to remove bubbles formed during mixing.

2. *PLA solution preparation*. PLA is a thermoplastic aliphatic polyester that is biodegradable under certain conditions, such as in the presence of oxygen. PLA has been employed in several biomedical applications, such as stents, sutures and tissue engineering scaffolds [24].

The PLA solution was prepared by dissolving PLA particles (Green Squire Material Co, Ltd) in acetone at a w/w ratio of 1 : 4, followed by stirring and shaking.

3. *Chitosan solution preparation*. Chitosan is a linear polysaccharide consisting of randomly distributed β-(1-4)-linked D-glucosamine (deacetylated unit) and *N*-acetyl-D-glucosamine (acetylated unit). It has been used in a number of commercial and biomedical applications [25, 26].

A chitosan solution (1.5 wt% (w/w)) was produced by dissolving chitosan powder in an acetic acid (0.5 wt% (w/w)).

4. *Nanomolding of tissue engineering scaffold*. PLGA and PLA scaffolds were fabricated by casting the polymer solution on the nanostructured Ni mold. The mold and casting were then placed in an airtight vessel overnight to allow acetone to gradually evaporate and the polymer to solidify. Ethanol was then added to the vessel and left at room temperature for 10 min to remove the film from the mold.

For the chitosan scaffold, the chitosan solution was first cast on the nanostructured Ni mold. The mold and the cast chitosan film were then placed in a vessel and heated in an oven at 50 °C overnight to completely evaporate the water. An NaOH–NaCl aqueous solution (1 wt% NaCl in 0.1 M NaOH) was then added to the vessel and left at room temperature for 30 min to remove the film from the mold.

The nanostructured topology of the membrane was characterized by AFM.

2.3. Cell culture

Mouse fibroblast cells (L929s) were cultured on the scaffolds consisting of different nanohemisphere arrays to investigate the influence of nanohemisphere arrays on skin tissue regeneration.

1. *Cell culture*. L929s were kept in a low glucose Dulbecco's modified Eagle's medium (DMEM; GIBCO), containing 10% fetal bovine serum (GIBCO) and 1% antibiotic–antimycotic (GIBCO) in a 75 ml flask at 37 °C in 5% CO_2. The culture medium was renewed every other day. TrypLE Express (GIBCO) was used to treat cells for secondary culture.
2. Cell seeding on biodegradable membrane. Nanostructured scaffolds of 0.6 mm diameter were glued to the center of each well in a 96-well plate. The L929s were treated with TrypLE Express. The cell suspension was then diluted to 4×10^3 cells per 200 μl and seeded on the nanostructured scaffolds at 37 °C in 5% CO_2.

2.4. L929 morphology observation

The L929s were stained with 4′, 6-dimidino-2-phenylindole (DAPI) and phalloidin to observe the cell nucleus and actin. The cells were stabilized with 4% paraformaldehyde for 15 min. After this, a 0.5% (v/v) Triton X-100 solution in phosphate buffered saline (PBS) was used for cell perforation for 10 min. 1% bovine serum albumin was then added to block the non-specific positions for 30 min. The nucleus and actin labeling took a further 10 and 30 min, respectively. A fluorescence microscope (DMIL LED, Leica) was used to capture fluorescence images of the nucleus and skeleton.

2.5. Proliferation assay

The proliferation assay was performed with WST-1 cell proliferation reagent (BioVision Co). After culture, the medium was removed and the cultured cells were washed with PBS. 20 μl WST-1 reagent was mixed with 200 μl of culture medium, added to each sample, and incubated for 2 h at 37 °C, under a 5% CO_2 atmosphere. The samples were finally shaken for 1 min to ensure a complete mixing of the WST-1 product and the medium. This suspension was then poured into a new 96-well microplate. An ELISA reader (Tecan Group, Ltd) of 492 nm wavelength was used for the absorbance value measurements. All experiments were repeated thrice.

2.6. Enzyme-linked immunosorbent assay of collagen type I

A sandwich ELISA was used to detect the concentration of collagen type I along with a Mouse Type I Collagen Detection kit (Invitrogen, TW). The 96-well plate was first coated with a capture antibody and left overnight. 100 μl sample and standard solutions were then added to each well and left for 2 h. 100 μl of detection antibody was then added to each well and allowed to bind to the collagen type I protein for 2 h. 100 μl enzyme-linked secondary antibody was subsequently added to each well for 1 h. 100 μl of substrate was finally added to each well and converted by the enzyme to a detectable form by leaving for 30 min. 2 N sulfuric acid was used to stop the reaction. The optical density values were then measured at 492 nm by the ELISA reader.

2.7. Statistical analysis

All the data obtained were expressed as the mean plus or minus one standard deviation (mean $\pm$ SD) and analyzed using a two-tailed *t*-test (SAS Institute Inc.).

3. Results and discussion

3.1. Nanomold fabrication results

The Ni nanomolds were fabricated according to the procedure depicted in figure 1. For electroforming the Ni nanomolds, two types (oxalic and phosphoric acid etched) of modified barrier-layer surfaces of AAO membrane were fabricated (see SEM images in figures 2(a) and (b)). Because of the internal stress during anodization, the etchant etched out more alumina at the borders between the cells than at the cell surfaces; accordingly, an array of orderly hemispheric nanostructures was obtained. The diameter and height of the oxalic acid-etched hemispheric nanostructures are 165 and 29 nm, respectively, as indicated by the AFM images shown in figure 3(a). The diameter and height of the phosphoric acid-etched structures are 572 and 128 nm, respectively (figure 3(b)).

The cyclic voltammogram obtained from the CV test on the gold (Au) thin film deposited on the AAO template is shown in figure 4. By integrating the area under the reducing peak in figure 4, the total electric charge is 1.35 mC. Since a charge of 386 μC per 1 cm^2 of Au electrode is required to

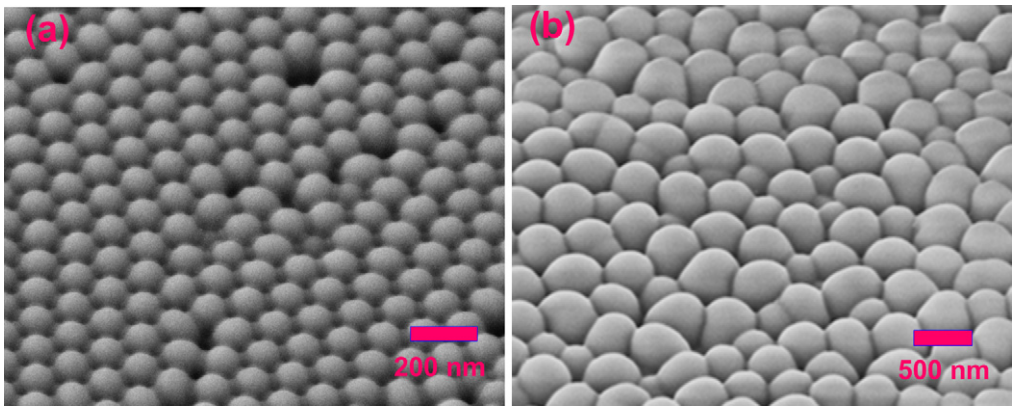

Figure 2. SEM images of the modified barrier-layer surfaces: (a) OA; and (b) phosphoric acid-etched AAO.

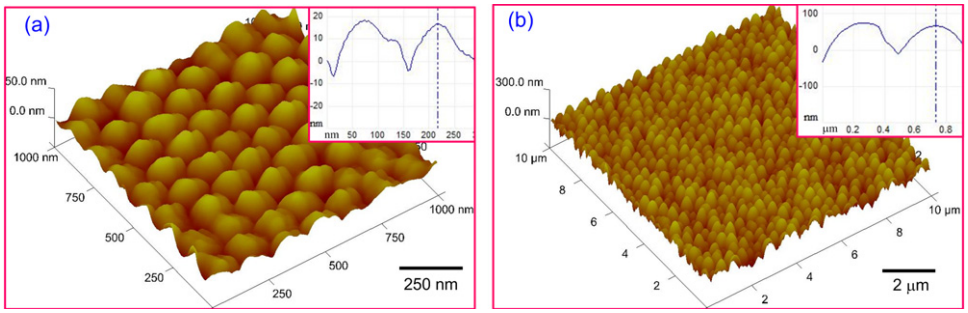

Figure 3. AFM images of the modified barrier-layer surfaces: (a) OA (scale bar = 250 nm); and (b) phosphoric acid-etched AAO (scale bar = 2 μm). The insets illustrate the height of the hemisphere.

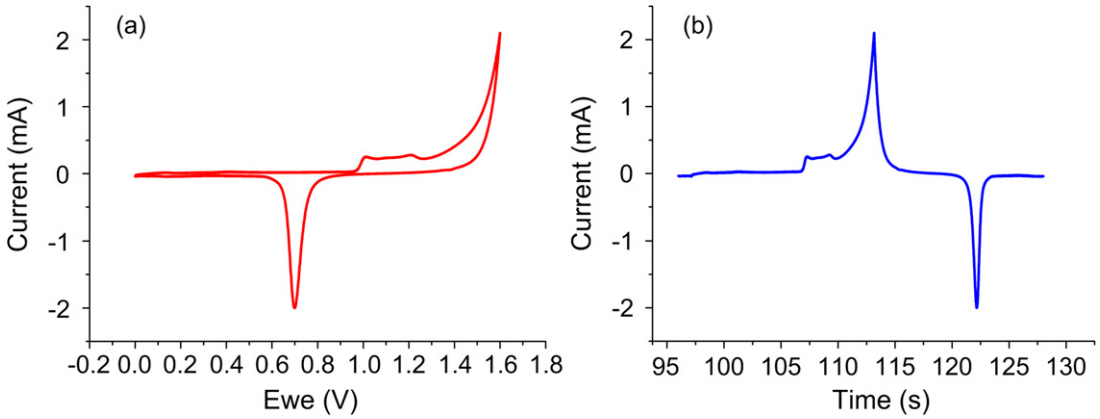

Figure 4. Cyclic voltammogram obtained from the CV test the gold (Au) thin film deposited on the AAO master mold: (a) *I–V* curve and (b) *I–t* curve.

form AuO, the effective area of the device was estimated to be 3.5 cm^2 (1.35 mC per 386 μC). In general, a 10 mA cm^{-2} current density is required for Ni deposition. Hence, a current of 35 mA was used for the deposition of the Ni thin film.

Figure 5 shows the SEM images of the Ni nanomolds obtained by electroforming. A concave nanostructure array was obtained. The average border-to-border length of an indent in the Ni mold, formed using an oxalic acid-etched AAO (OA) template, was determined to be approximately 142 nm with a depth of 28 nm, from the AFM image shown in the inset of figure 5(a). The average border-to-border length and depth of an indent in the Ni mold, formed using a phosphoric acid-etched AAO template, are 445 and 86 nm, respectively (inset of figure 5(b)). In both cases, the border-to-border length is larger than the diameter of the nanohemispheres on the AAO master mold, while the depth is less than the height of the nanohemispheres. This is because the Ni ions cannot completely fill the area between the nanohemispheres on the AAO master mold during electroforming. To obtain well-defined nanohemisphere arrays, barrier-layer side etching for a longer time may be required.

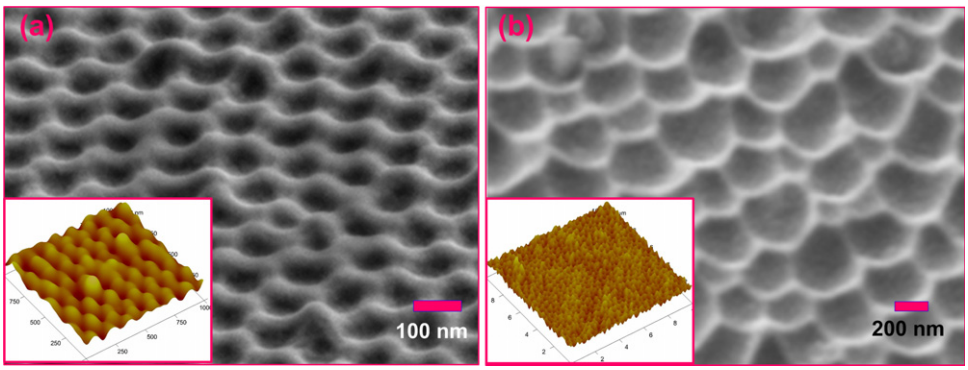

Figure 5. SEM images of the electroformed nickel nanomold formed from: (a) OA template (scale bar = 100 nm); and (b) phosphoric acid-etched AAO template (scale bar = 200 nm), the insets are the AFM images.

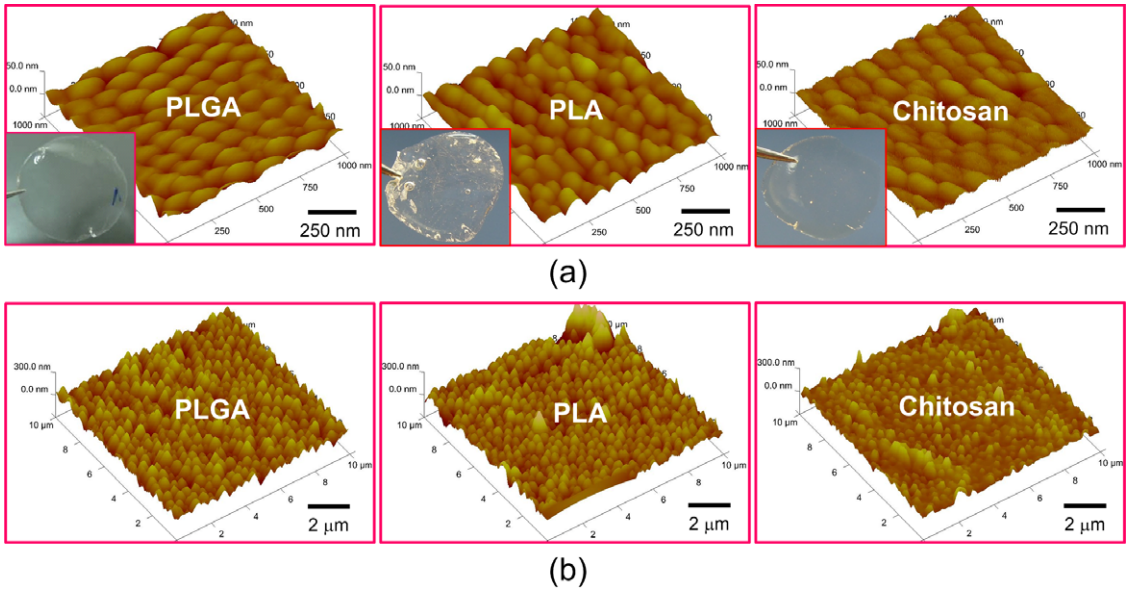

Figure 6. Polymer scaffolds formed from the nickel nanomolds from: (a) OA templates (scale bar = 250 nm); and (b) phosphoric acid-etched AAO templates (scale bar = 2 μm). The insets are the OM images.

3.2. Nanostructured biodegradable scaffold casting

AFM images of the nanopatterned scaffolds obtained by replica casting are shown in figure 6. From the AFM images, it can be observed that the hemispheric nanostructures on all three biodegradable materials are evenly distributed. This suggests that our nanostructure mold might be a practicable tool for the mass production of nanopatterned biodegradable scaffolds for tissue engineering. SEM images of the scaffolds were also acquired, however, damage occurred at high magnifications.

Table 1 summarizes the measurement data of the AAO templates, Ni nanomolds and scaffold casting results. For those scaffolds cast using the oxalic-acid-based nanomold, the average heights of the nanohemispheres in the PLGA, PLA and chitosan scaffolds are 21 ± 1, 15 ± 2 and 25 ± 2 nm, respectively. It is presumed that the variation in the viscosity of the polymeric materials results in differences in the rate at which the solution fills the concave nanohemispheres of the Ni nanomold. The intrinsic viscosity (IV) of PLGA, PLA and chitosan are 0.43, 0.63 and 0.15 dl g^{-1}, respectively. By comparing the scaffold feature depth to the 28 ± 1 nm depth of the nanohemisphere in the oxalic-acid-based Ni nanomold, the filling rate of PLGA, PLA and chitosan can be estimated as 77, 53 and 90%, respectively. The surface roughness (R_a) in the PLGA, PLA and chitosan scaffolds are 4.3, 4.4 and 3.8 nm, respectively. The roughness of the flat PLGA and PLA is similar. It is about 4 nm. These roughness values are lower than the surface roughness of the mold from which the scaffolds were cast. This indicates that the concave nanohemispheres of the Ni nanomold were not completely filled by the material solution during casting.

The casting results using the phosphoric acid-based nanomolds are similar to the oxalic acid ones. Since the dimensions of the OA templates are three- to four-fold smaller to those of the phosphoric acid ones, this is reflected in the height, diameter and surface roughness values.

Table 1. Comparison of the height, diameter and R_a for the AAO template, Ni nanomold and polymer scaffolds.

	AAO	Ni mold	PLGA	PLA	Chitosan
Oxalic acid-etched AAO					
Height (nm)	29 ± 1	28 ± 1	21 ± 1	15 ± 2	25 ± 2
Diameter (nm)	165 ± 5	142 ± 2	119 ± 6	117 ± 11	118 ± 9
R_a (nm)	6.7	5.9	4.3	4.4	3.8
Phosphoric acid-etched AAO					
Height (nm)	128 ± 27	86 ± 10	87 ± 6	72 ± 2	66 ± 8
Diameter (nm)	572 ± 65	445 ± 127	533 ± 43	491 ± 55	486 ± 54
R_a (nm)	32.1	21.5	32.4	30.2	23.2

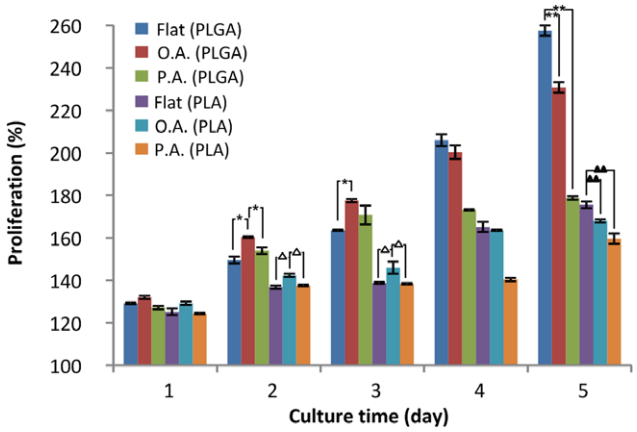

Figure 7. L929 proliferation on different nanostructured scaffolds for 5 d. An asterisk denotes OA scaffold versus flat scaffold and PA scaffold on PLGA, $p < 0.05$. Triangle denotes OA scaffold versus flat scaffold and PA scaffold on PLA, $p < 0.05$. A double asterisk denotes flat scaffold versus OA scaffold and PA scaffold on PLGA, $p < 0.05$. A double triangle denotes flat scaffold versus OA scaffold and PA scaffold on PLA, $p < 0.05$.

3.3. Cell proliferation on different scaffold materials at different culture times

Nanostructures can enhance cell proliferation if the features are below a certain size [27, 28]. Since a biodegradable scaffold will degrade during the culture time, the nanostructure of this biodegradable scaffold will also change. Therefore, the cell proliferation on different scaffold materials, with various nanohemisphere sizes, at different culture times was investigated. Figure 7 presents the 5 d culture results of L929. Since the chitosan scaffold tends to swell in the early stage of culture, differences in the cell proliferation on these scaffolds with increasing culture time were not apparent and are omitted from this graph.

On day one, no obvious proliferation difference within or between the PLGA and PLA samples is observed. After 2 d of culture (day two and day three), the scaffolds fabricated using a nickel nanomold from the OA template show more improved cell proliferation than the flat scaffolds and the scaffolds from the phosphate acid-etched AAO (PA) template. The cell proliferation on the flat scaffolds dramatically increases after 4 d of culture. Figure 7 also shows that PLGA is better than PLA in promoting the growth of L929.

The cell adhesion process can be divided into three steps: these include rolling on the material surface, cell membrane ligands adhering to the scaffold surface and cell extension. In general, it takes 4–24 h for the cell to firmly attach to a scaffold [29]. On the first day of culture, most of the cells are still suspended in the culture medium or initially rest on the scaffold surface. Therefore, no notable proliferation difference is observed. On day two, the cell senses the nanostructure on the scaffold surface, and the proliferation-related pathways such as MAP kinase (ERK1/2) and Akt are activated to enhance cell growth [30]. After 3 d of culture, the influence of the nanostructure on cell proliferation gradually diminishes due to environmental conditions (pH condition, cell metabolism) inducing material swelling or causing degradation [31]. It can therefore be concluded that the nanostructure has a higher potential to shorten the proliferation step of the wound-healing process when cells are cultured on it for 2 or 3 d.

3.4. Size effect of the nanostructure on cell proliferation

As tabulated in table 1, the roughness values of the OA scaffold and the PA scaffold are 4 and 30 nm, respectively. However, the hemisphere diameters of the OA scaffold and the PA scaffold are 120 and 500 nm, respectively. The OA and PA differ significantly in both diameter and roughness. In addition to the size effect, surface roughness is the other important effect on fibroblast proliferation. The lower roughness may have an effect on fibroblast proliferation such as in the flat scaffolds as well as the OA scaffolds. However, the proliferation of fibroblasts on PA scaffolds is likely to be influenced by surface roughness. It has been reported that the proliferation of fibroblasts decreases with an increase in surface roughness [32]. Since the surface roughness of PA scaffolds is much larger than that of the OA scaffolds, the proliferation of fibroblasts on PA scaffolds was not as good as that on OA scaffolds.

As already discussed, the proliferation of L929 is promoted by the nanostructured scaffold after 2 d of culture. Further investigation is therefore warranted to determine any size effect of the nanostructure on cell proliferation to more accurately gauge the effect on wound-healing time.

Figure 8 shows the fluorescence images of the nucleus and skeleton of L929 on different nanostructure scaffolds after 2 d of culture. The original spindle-like morphology of the cells is shown in figures 8(a) and (b). When an OA scaffold is used, the morphology of the cells changes to become more extended and elongated (figures 8(c) and (d)). The cell shape

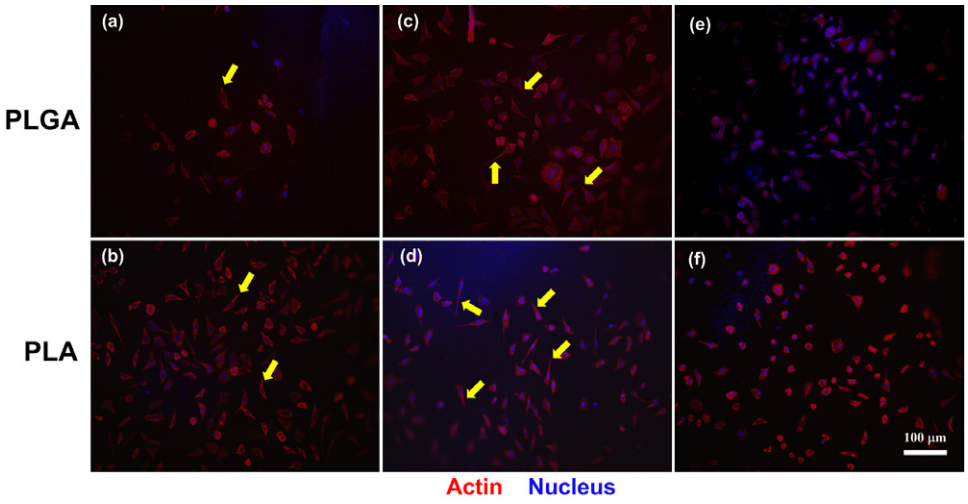

Figure 8. L929 morphology on different nanostructured scaffolds after 2 d of culture. (a), (b) flat scaffold; (c), (d) OA scaffold; and (e), (f) PA scaffold. The elliptical and speckled nucleus are indicated by the arrowheads.

when cultured on PA scaffolds is more circular and the cells are smaller (figures 8(e) and (f)).

Fibroblast and fibrocyte are two states of the same cell. The fibroblast is the activated state and fibrocyte is the less active state. In the activated state, the elliptical and speckled nucleus (as indicated by the yellow arrowheads in figure 8) with two or more nucleoli is surrounded by the branched cytoplasm. Therefore, active fibroblasts can be identified by their abundant rough endoplasmic reticulum. For the cells cultured on OA scaffolds, cytoplasm with abundant branches is observed when compared to other scaffolds. This observation shows that the OA scaffolds possess a higher potential to activate the fibroblasts.

In general, the influence of a micro-scale scaffold on cell growth is the structure of the scaffold [33]. However, the influence of a nanoscale scaffold is that its nanostructure can induce the cultured cells to outstretch their pseudopodium and adhere to the scaffold surface [34]. This study belongs to the latter scope. The fluorescence images of the nucleus and skeleton shown in figure 8 confirm that L929 grew non-directionally.

Figure 9 compares the proliferation of L929 on different scaffolds after 2 d of culture. Each experiment was repeated five times ($n = 5$). The results indicate that the scaffolds from the OA template are better at promoting L929 proliferation than the other scaffolds.

It has been reported that fibroblasts prefer to grow on rougher and more hydrophilic surfaces [28]. Another study, however, has shown that the proliferation of fibroblasts decreases with an increase in surface roughness [32]. Further studies have observed that fibroblasts prefer to be cultured on a nanostructured surface of hemispheres with a diameter of 80–100 nm [27, 28]. In this study, we have demonstrated that the proliferation of L929 is aided when a nanostructured PLGA scaffold of uniform hemisphere array with the diameter of the hemisphere being 118 nm is employed.

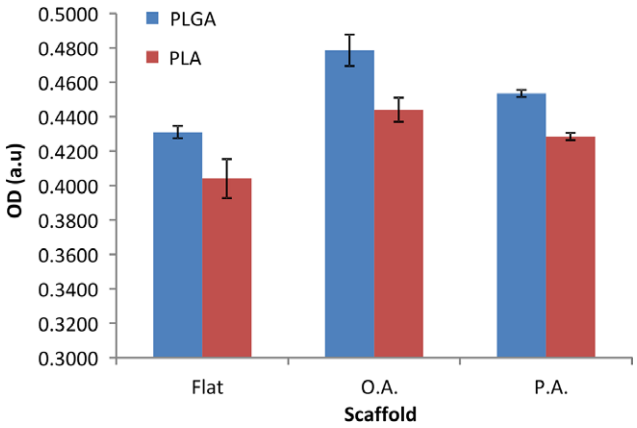

Figure 9. L929 proliferation on different nanostructured scaffolds after 2 d of culture.

3.5. Influence of nanostructure on collagen type I production

Collagen plays an important role in scar formation of the tissue remodeling step. During the wound-healing process, the fibroblasts will proliferate and secrete collagen type I to fill the wound. However, when collagen is abnormally secreted, unwanted keloid is produced simultaneously. It is a result of an overgrowth of granulation tissue (collagen type III) at the site of a healed skin injury which is then slowly replaced by collagen type I [35, 36]. Since nanostructures tend to enhance the proliferation of fibroblasts, it is therefore important to study the effect of nanostructures on collagen type I production.

Figure 10 shows the concentration of collagen type I of L929 cultured on different scaffolds. Similar to the cell proliferation results, the L929 cultured on the nanostructured PLGA scaffolds fabricated using a nanonickel mold from the OA template secreted more collagen type I than that of the other scaffolds.

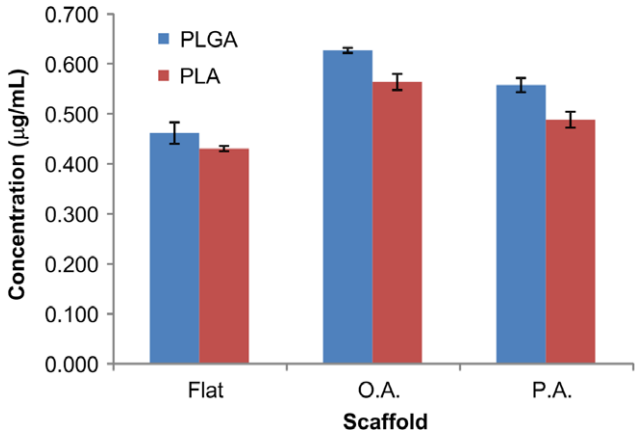

Figure 10. Collagen type I assay on different scaffolds.

It is well known that nanofibers have good wound-healing and tissue-regeneration abilities. Tysseling-Mattiace *et al* [37] have used nanofibers to inhibit glial scar formation and promote axon elongation after spinal cord injury. Compared to other nanofiber-based scaffolds, the nanostructured scaffolds presented in this study can be mass produced relatively easily.

4. Conclusion

Skin serves as a protective barrier, modulating body temperature and waste discharge; because of this, any laceration or wound should be repaired as soon as possible. The ability to control the proliferation of skin cells and the extracellular matrix of the cells is a crucial issue in skin-regeneration research. In this study, the influence of nanostructured scaffolds consisting of nanohemisphere arrays on skin tissue regeneration was investigated. Nanostructured tissue engineering scaffolds of PLGA, PLA and chitosan were synthesized and mouse fibroblast cells (L929s) were cultured to investigate any effect on cell proliferation. The experimental results demonstrate that the proliferation of L929 is best enhanced when a nanostructured PLGA scaffold, consisting of a uniform hemisphere array with a feature diameter of 118 nm is employed.

Acknowledgment

The authors thank the National Science Council of Taiwan under grant number NSC-100-2221-E-005-014-MY3 for their financial support of this research.

References

[1] Martin P 1997 Wound healing—aiming for perfect skin regeneration *Science* **276** 75–81
[2] Zhou Y, Yang D, Chen X, Xu Q, Lu F and Nie J 2007 Electrospun water-soluble carboxyethyl chitosan/poly(vinyl alcohol) nanofibrous membrane as potential wound dressing for skin regeneration *Biomacromolecules* **9** 349–54
[3] Velnar T, Bailey T and Smrkolj V 2009 The wound healing process: an overview of the cellular and molecular mechanisms *J. Int. Med. Res.* **37** 1528–42
[4] Kukumberg M, Lim W J, Yamamoto M and Yim E K F 2012 Nano and microtopography enhance differentiation of human mesenchymal stem cell into endothelial-like cells for vascular repair *J. Tissue Eng. Regen. Med.* **6** 143–4
[5] Pan H-A *et al* 2009 A nanodot array modulates cell adhesion and induces an apoptosis-like abnormality in NIH-3T3 cells *Nanoscale Res. Lett.* **4** 903–12
[6] Xia L *et al* 2012 *In vitro* and *in vivo* studies of surface-structured implants for bone formation *Int. J. Nanomed.* **7** 4873–81
[7] Chandrasekaran A R, Venugopal J, Sundarrajan S and Ramakrishna S 2011 Fabrication of a nanofibrous scaffold with improved bioactivity for culture of human dermal fibroblasts for skin regeneration *Biomed. Mater.* **6** 015001
[8] Zhaoa C, Tan A, Pastorin G and Ho H K 2013 Nanomaterial scaffolds for stem cell proliferation and differentiation in tissue engineering *Biotechnol. Adv.* **31** 654
[9] Park K S *et al* 2012 Mass-producible nano-featured polystyrene surfaces for regulating the differentiation of human adipose-derived stem cells *Macromol. Biosci.* **12** 1480–9
[10] Gates B D, Xu Q, Stewart M, Ryan D, Willson C G and Whitesides G M 2005 New approaches to nanofabrication: molding, printing and other techniques *Chem. Rev.* **105** 1171–96
[11] Teo B and Sun X 2006 From top-down to bottom-up to hybrid nanotechnologies: road to nanodevices *J. Cluster Sci.* **17** 529–40
[12] Barth J V, Costantini G and Kern K 2005 Engineering atomic and molecular nanostructures at surfaces *Nature* **437** 671–9
[13] Chou S Y, Krauss P R and Renstrom P J 1996 Imprint lithography with 25-nanometer resolution *Science* **272** 85–7
[14] Guo L J 2007 Nanoimprint lithography: methods and material requirements *Adv. Mater.* **19** 495–513
[15] Zankovych S, Hoffmann T, Seekamp J, Bruch J and Torres C S 2001 Nanoimprint lithography: challenges and prospects *Nanotechnology* **12** 91
[16] Hong S-H, Bae B-J, Hwang J-Y, Hwang S-Y and Lee H 2009 Replication of high ordered nano-sphere array by nanoimprint lithography *Microelectron. Eng.* **86** 2423–6
[17] Zhao S, Roberge H, Yelon A and Veres T 2006 New application of AAO template: a mold for nanoring and nanocone arrays *J. Am. Chem. Soc.* **128** 12352–3
[18] Zhou W *et al* 2009 Porous alumina nano-membranes: soft replica molding for large area UV-nanoimprint lithography *Microelectron. Eng.* **86** 2375–80
[19] Wang G-J, Lin Y-C, Li C-W, Hsueh C-C, Hsu S-H and Hung H-S 2009 Fabrication of orderly nanostructured PLGA scaffolds using anodic aluminum oxide templates *Biomed. Microdevices* **11** 843–50
[20] Kumar G, Tang H X and Schroers J 2009 Nanomoulding with amorphous metals *Nature* **457** 868–72
[21] Veith M *et al* 2010 Adhesion of fibroblasts on micro- and nanostructured surfaces prepared by chemical vapor deposition and pulsed laser treatment *Biofabrication* **2** 035001
[22] Choi C-H and Kim C-J 2012 Advanced nanostructured surfaces for the control of biofouling: cell adhesions to three-dimensional nanostructures *Green Tribology* ed M Nosonovsky and B Bhushan (Berlin: Springer) pp 79–103
[23] Sionkowska A 2011 Current research on the blends of natural and synthetic polymers as new biomaterials: review *Prog. Polym. Sci.* **36** 1254–76
[24] Middleton J C and Tipton A J 2000 Synthetic biodegradable polymers as orthopedic devices *Biomaterials* **21** 2335–46

[25] Wittmer C R, Phelps J A, Lepus C M, Saltzman W M, Harding M J and Van Tassel P R 2008 Multilayer nanofilms as substrates for hepatocellular applications *Biomaterials* **29** 4082–90
[26] Pavinatto F J, Caseli L and Oliveira O N Jr 2010 Chitosan in nanostructured thin films *Biomacromolecules* **11** 1897–908
[27] Kim D H *et al* 2005 Cellular responses to nanotopology of polymeric surfaces fabricated with AAO nanoimprinting *3rd IEEE/EMBS Special Topic Conf. on Microtechnology in Medicine and Biology, 2005* pp 188–9
[28] Dalby M J, Riehle M O, Sutherland D S, Agheli H and Curtis A S G 2004 Changes in fibroblast morphology in response to nano-columns produced by colloidal lithography *Biomaterials* **25** 5415–22
[29] Prabhakarpandian S M B, Pant K and Kiani M F 2011 Microfluidic device for modeling cell–cell and particle–cell interactions in the microvasculatre *Microvasc. Res.* **8** 210–20
[30] Kasaj A, Willershausen B, Reichert C, Gortan-Kasaj A, Zafiropoulos G G and Schmidt M 2008 Human periodontal fibroblast response to a nanostructured hydroxyapatite bone replacement graft *in vitro Arch. Oral Biol.* **53** 683–9
[31] Yoo J Y, Kim J M, Seo K S, Jeong Y K, Lee H B and Khang G 2005 Characterization of degradation behavior for PLGA in various pH condition by simple liquid chromatography method *Biomed. Mater. Eng.* **15** 279–88
[32] Kunzler T P, Drobek T, Schuler M and Spencer N D 2007 Systematic study of osteoblast and fibroblast response to roughness by means of surface-morphology gradients *Biomaterials* **28** 2175–82
[33] He X L, Nie P P, Chen B Z, Li X X, Chen L, Guo G and Zhang R 2012 A novel method to fabricate thermoresponsive microstructures with improved cell attachment/detachment properties *J. Biomed. Mater. Res.* A **100** 1946–53
[34] Choi C H, Heydarkhan-Hagvall S, Wu B M, Dunn J C Y, Beygui R E and Kim C J 2009 Cell growth as a sheet on three-dimensional sharp-tip nanostructures *J. Biomed. Mater. Res.* A **89** 804–17
[35] Ogawa R 2010 The most current algorithms for the treatment and prevention of hypertrophic scars and keloids *Plast. Reconstr. Surg.* **125** 557–68
[36] Rockwell W B, Cohen I K and Ehrlich H P 1989 Keloids and hypertrophic scars—a comprehensive review *Plast. Reconstr. Surg.* **84** 827–37
[37] Tysseling-Mattiace V M *et al* 2008 Self-assembling nanofibers inhibit glial scar formation and promote axon elongation after spinal cord injury *J. Neurosci.* **28** 3814–23